



Time-Dependent Biosensor Fluorescence as a Measure of Bacterial Arsenic Uptake Kinetics and Its Inhibition by Dissolved Organic Matter

Hyun Yoon, Andrea Giometto, Martin P. Pothier, Xuhui Zhang, Alexandre J. Poulain, Matthew C. Reid

^aSchool of Civil and Environmental Engineering, Cornell University, Ithaca, New York, USA ^bDepartment of Biology, University of Ottawa, Ottawa, Ontario, Canada

ABSTRACT Microbe-mediated transformations of arsenic (As) often require As to be taken up into cells prior to enzymatic reaction. Despite the importance of these microbial reactions for As speciation and toxicity, understanding of how As bioavailability and uptake are regulated by aspects of extracellular water chemistry, notably dissolved organic matter (DOM), remains limited. Whole-cell biosensors utilizing fluorescent proteins are increasingly used for high-throughput quantification of the bioavailable fraction of As in water. Here, we present a mathematical framework for interpreting the time series of biosensor fluorescence as a measure of As uptake kinetics, which we used to evaluate the effects of different forms of DOM on uptake of trivalent arsenite. We found that thiolcontaining organic compounds significantly inhibited uptake of arsenite into cells, possibly through the formation of aqueous complexes between arsenite and thiol ligands. While there was no evidence for competitive interactions between arsenite and low-molecularweight neutral molecules (urea, glycine, and glyceraldehyde) for uptake through the aquaglyceroporin channel GlpF, which mediates transport of arsenite across cell membranes, there was evidence that labile DOM fractions may inhibit arsenite uptake through a catabolite repression-like mechanism. The observation of significant inhibition of arsenite uptake at DOM/As ratios commonly encountered in wetland pore waters suggests that DOM may be an important control on the microbial uptake of arsenite in the environment, with aspects of DOM quality playing an important role in the extent of inhibition.

IMPORTANCE The speciation and toxicity of arsenic in environments like rice paddy soils and groundwater aquifers are controlled by microbe-mediated reactions. These reactions often require As to be taken up into cells prior to enzymatic reaction, but there is limited understanding of how microbial arsenic uptake is affected by variations in water chemistry. In this study, we explored the effect of dissolved organic matter (DOM) quantity and quality on microbial As uptake, with a focus on the role of thiol functional groups that are well known to form aqueous complexes with arsenic. We developed a quantitative framework for interpreting fluorescence time series from whole-cell biosensors and used this technique to evaluate effects of DOM on the rates of microbial arsenic uptake. We show that thiol-containing compounds significantly decrease rates of As uptake into microbial cells at environmentally relevant DOM/As ratios, revealing the importance of DOM quality in regulating arsenic uptake, and subsequent biotransformation, in the environment.

KEYWORDS arsenic, microbial uptake, bioavailability, biosensors, kinetics, dissolved organic matter, thiols, arsenite, complexation, modeling

rsenic (As) is a ubiquitous environmental toxin with major impacts on human and ecosystem health (1–5). Microbe-mediated transformations influence As speciation, fate, and transport, and there is great interest in the role of these processes in the

Editor Jennifer B. Glass, Georgia Institute of Technology

Copyright © 2022 American Society for Microbiology. All Rights Reserved.

Address correspondence to Matthew C. Reid, mcr239@cornell.edu.

The authors declare no conflict of interest.

Received 31 May 2022 Accepted 11 July 2022 Published 1 August 2022

Downloaded from https://journals.asm.org/journal/aem on 12 September 2022 by 128.84.126.165.

biogeochemical cycling of As in aquatic environments like rice paddies and ground-water aquifers (6–8). In rice paddies, for example, root uptake and the toxicity of As accumulating in rice grains depend on microbially mediated redox and methylation-demethylation reactions that control As speciation in the rhizosphere (9–12). Many of these reactions are mediated by intracellular As metabolism enzymes (8, 13, 14), so the first step for these reactions is uptake across cellular membranes into cells. Uptake of arsenate [As(V)] into cells is facilitated by phosphate transporters (15–18), while As(III) uptake is regulated by the glycerol facilitator protein GlpF (19–21). GlpF is an aquagly-ceroporin containing size and charge selectivity filters (22, 23) which regulates the transport of water and low-molecular-weight (LMW) organic molecules with net neutral charges, including glycerol, urea, glycine, and glyceraldehyde, across the cytoplasmic membrane (24–26). Arsenite [As(III)] (pK_{a1} = 9.2) is primarily uncharged at circumneutral pH (see Fig. S1 in the supplemental material) (27), which allows it to be taken up through GlpF channels.

There is growing interest in the effects of different extracellular water chemistries on As uptake into microbial cells. While phosphate is known to inhibit uptake of As(V) through a competitive inhibition mechanism (17), the effects of dissolved organic matter (DOM) quantity and quality on As uptake are not well understood. This is a notable knowledge gap, since rice paddy soils and other environments with mobilized As are often characterized by high levels of DOM (28, 29). It is known that glucose can inhibit uptake of As(III) via catabolite repression on GlpF in bacteria (30), but other mechanisms for DOM influence on microbial As uptake have not been thoroughly investigated. For example, As(III) forms aqueous complexes with DOM (31-34), a process known to affect bioavailability and biotransformation of other elements, notably, mercury (35–38). While a range of mechanisms of binding of As(III) to DOM have been discussed (39, 40), there is growing evidence that thiol functionalities are key binding sites for As(III) (41-44), consistent with well-known interactions between As(III) and thiols in cysteine residues of proteins (45, 46) and phytochelatins (47). The effects of such As(III)-DOM complexation on microbial uptake, and subsequent biotransformation, of As are not fully understood. It is also not clear whether LMW organic molecules that are taken up through GlpF transporters can inhibit the uptake of As(III) through the same channel.

Two approaches are commonly used to quantify As uptake into bacterial cells. The first approach uses inductively coupled plasma mass spectrometry (ICP MS) quantification of dissolved As with mass balance methods to estimate microbial uptake. Since both intracellular uptake and biosorption onto cellular membranes or cell debris in the media remove As from the aqueous phase (48), it can be difficult to distinguish intracellular uptake from other processes using this approach. Rapid extrusion of As(III) via efficient ArsB As(III) efflux pumps (49) can further limit the effectiveness of mass balance methods. The second approach involves the use of whole-cell biosensors that express fluorescent proteins (e.g., green fluorescent protein or mCherry) in the presence of intracellular As (50, 51). In a previous study, we introduced a whole-cell Escherichia coli biosensor with the mCherry reporter gene downstream of the arsenicsensitive arsR transcriptional repressor, which is known to be specific to only As and antimony (Sb) (52, 53). The ArsR bioreporter circuit is a negative-feedback system, so evaluating functional relationships between intracellular As(III) and/or As(III) uptake rates and biosensor fluorescence is highly complex (54). Biosensor methods have usually used endpoint fluorescence measurements to determine As bioavailability (50, 55), and when fluorescence time series have been used, they have not been explicitly linked to uptake kinetics (50, 56), with the exception of the work of Berset et al. (54), in which the fluorescence production was fit to a mechanistic model, whose complexity might limit its applicability. In this study, we introduced a novel mathematical framework to evaluate microbial As uptake kinetics from fluorescence time series in the ArsR-based bioreporter circuit, which may allow for novel inferences into processes controlling As uptake.

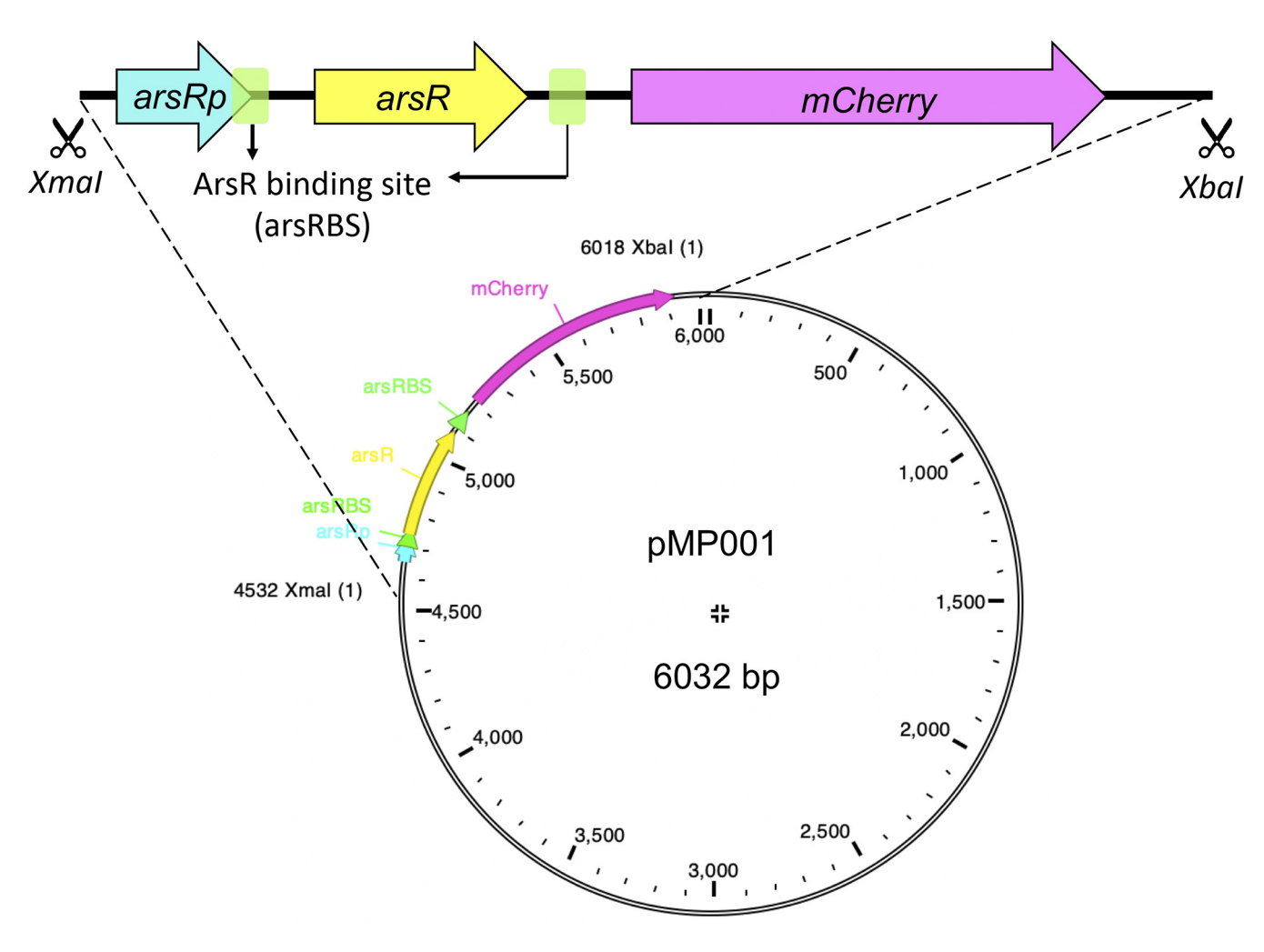


FIG 1 Graphic map of the reporter construct inserted in the pUCP19 vector. The map was obtained using ApE software (https://jorgensen.biology.utah.edu/wayned/ape/) after annotating fragments with the pLannotate web-based service (96). Intracellular As(III) binds to ArsR and induces the expression of arsR and the subsequent mCherry reporter gene. Any potential inhibitors reduce fluorescence indicating less As(III) uptake.

The objective of this research was to explore the effects of DOM on microbial As(III) uptake, with a specific focus on the effects of As(III) complexation with thiol ligands, using the kinetics-based interpretation of biosensor fluorescence data. We developed mathematical equations to relate fluorescence time series to As uptake rates. Using this approach for interpreting fluorescence time series, we evaluated the effect of LMW organic molecules and thiol-containing molecules, including a thiol-rich DOM, on As uptake kinetics.

RESULTS

Model development. The principle for the biosensor is that binding of intracellular As(III) to the ArsR As(III)-responsive DNA binding transcriptional repressor allows for induction of the *ars* promoter (*arsRp*) and expression of the downstream *mCherry* gene (Fig. 1). Because induction of the *ars* promoter also leads to expression of the *arsR* gene, this is a negative-feedback system. In this study, we developed and tested a phenomenological model describing the rate of change of biosensor fluorescence (i.e., dF_{RFU}/dt , where F_{RFU} is biosensor fluorescence) as a function of intracellular As concentrations and used this model to determine and compare As uptake kinetics using the time series of biosensor fluorescence data. A more comprehensive mechanistic model for regulation of fluorescent protein dynamics in As-sensitive bioreporters has been described previously (54) and provides useful insights into the complex dynamics of the negative-feedback system governing fluorescent protein production. However, this

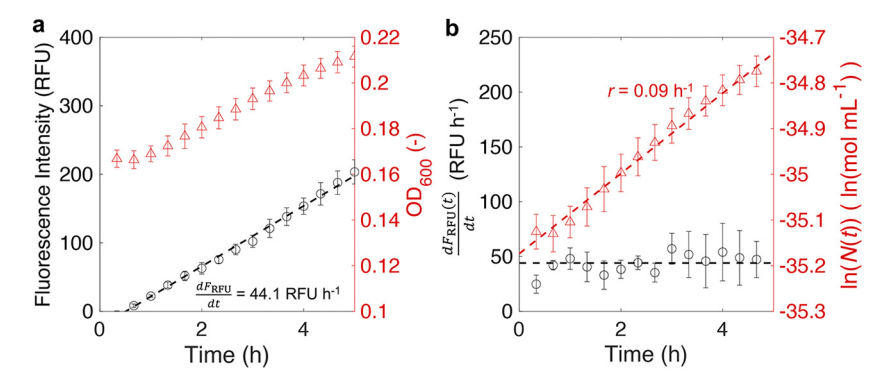


FIG 2 Illustration of the determination of As(III) uptake rates based on biosensor fluorescence time series data. (a) Measured fluorescence intensities (circles) and OD_{600} (triangles) during a representative biosensor assay. The linear regression line (black dashed line) was fit to the measured fluorescence data. (b) $dF_{RFU}(t)/dt$ (circles) and In(N(t)) (triangles) over time. The linear regression line (red dashed line) was fit to N(t) data converted from measured OD_{600} data through a calibration curve based on a serial dilution assay. The black dashed line represents the slope of the regression line (44.1 RFU h⁻¹) in panel a.

earlier model does not account for cell growth and has a very large number of fit parameters which are difficult to estimate with experimental data. These factors make the parameterization and application of this model a challenge under realistic conditions. Our more parsimonious model is advantageous because it can be parameterized with a relatively small number of measurements, reducing the chances of overfitting and making the model easier to apply.

A complete derivation of our model is described in Materials and Methods. The derivation results in the following equation describing the cellular As uptake rate:

$$\mu(t) \equiv \sqrt{\frac{1}{N(t)}} \frac{dF_{\rm RFU}}{dt} \sqrt{\frac{P_N}{\gamma}} \sqrt{\beta} - 4r P_N = \Psi(t) \sqrt{\frac{P_N}{\gamma}} \sqrt{\beta} - 4r P_N$$
 (1)

where $\mu(t)$ is the net As(III) uptake rate per cell at time t (moles per mole per hour), F_{RFU} is the measured fluorescence intensity (relative fluorescence units [RFU]), P_N is the average plasmid copy number per cell (moles per mole), γ is fluorescence per molar concentration of mCherry protein (RFU per milliliter per mole), β is the rate of transcription/translation of ArsR per ars promoter (per hour), and r is the first-order growth rate (per hour). $\Psi(t)$ is then introduced as a lumped parameter for $\sqrt{\frac{1}{N(t)}} \frac{dF_{\text{RFU}}}{dt}$, that is proportional to the uptake rate for convenience ($\sqrt{\text{RFU}}$ mL mol $^{-1}$ h $^{-1}$). Equation 1 shows that the log value of the slope of $F_{\text{RFU}}(t)$ normalized by cell number can be used for determining variations in the As(III) uptake rate $\mu(t)$, if all other variables are equal. In some cases the first-order growth rate r was shown to vary between experimental conditions, and in these cases r is estimated by fitting cell numbers converted from optical density at 600 nm (OD₆₀₀) (Fig. 2; see also Fig. S2 in the supplemental material) to determine its impact on $\mu(t)$. P_N and β are constants that can be estimated from previous studies (Table 1). The constant γ converts the molar concentration of mCherry to measurable RFU.

The constant γ is not available in our study since it requires quantification of mCherry protein, which is beyond the scope of this work. However, using measured values of dF_{RFU}/dt and N(t) at 5 h, and r (Fig. 2) from biosensor measurements, $\mu(t)$ from different conditions can be compared on a semiquantitative basis, enabling evaluation of effects of inhibitors since γ will be constant across all conditions. For dF_{RFU}/dt at 5 h, the slope of F_{RFU} over 5 h was used since F_{RFU} linearly increases over the first 5 h. To smooth the data, $F_{\text{RFU}}(t)$ and N(t) measurements were fit with a linear and exponential model, respectively, using the *fitnlm* function in MATLAB (MathWorks Inc., Natick, MA). In each case, the curve with the highest r^2 value ($r^2 > 0.99$) was selected (Fig. 2a).

Validation of plate reader-based fluorescence data with microscopy. Quantitative analysis of fluorescence micrographs was used to evaluate the distribution of single-

TABLE 1 Parameters used for determining As uptake kinetics from biosensor fluorescence

Parameter	Range of values	Description
$\overline{P_N}$	0–60 mol mol ⁻¹	Expected to be less than the previously reported copy no. of pUC19 vector in E . coli NEB 10-beta (60 mol mol ⁻¹) (98) due to its extended length by insertion of gene construct
β	43.2-50.4 h ⁻¹	Total transcription/translation rate estimated by using parameters from the work of Berset et al.
		(54); $\beta = \frac{1}{\frac{1}{k_m} + \frac{1}{k_p}}$, where k_m and k_p are transcription and translation rates, respectively. k_m of
		arsR and mCherry under the control of the same promoter are equal to 0.015 s ⁻¹ . k_p of arsR and gfp were 0.073 s ⁻¹ and 0.184 s ⁻¹ , respectively. k_p of mCherry was assumably equal to k_p of gfp based on the previous report (99).
F_{RFU}	0-1,000 RFU	Measured
r	0.082-0.155 h ⁻¹	Measured
N(t)	$0.43 \times 10^{-15} 1.29 \times 10^{-15} \text{mol mL}^{-1}$	Converted from measured OD ₆₀₀ through a calibration curve (Fig. S3)

cell fluorescence intensities and to assess whether attenuation of fluorescence by DOM could impact fluorescence measurements by the plate reader. Unexpectedly, 50 to 60% of cells were fluorescent below the limit of quantification (LOQ) for all As(III) concentrations (LOQ, <100 RFU [Fig. 3a]). Peaks in the distribution of fluorescence intensities at 20 h shifted to higher values as the As(III) concentration increased. The mean fluorescence intensities were 78.88, 149.63, 160.75, and 186.25 RFU for 400, 800, 1,600, and 3,200 nM As(III), respectively. Microscopy-based mean fluorescence intensities were strongly correlated with plate reader-based As(III) uptake rates at the same As(III) concentrations (r = 0.98 [Fig. 3c]).

To assess whether the nonfluorescing cells observed in Fig. 3 could be due to inactive cells in the late stationary or death phase of the *E. coli* culture at 20 h, time series measurements were obtained with the biosensor incubated with a fixed As(III) concentration (3,200 nM). Peaks in the fluorescence intensity distribution shifted to higher values as time increased. The ratio of nonfluorescent cells remained similar (50.8 to 58.0%) (Fig. S3), however, indicating that the lack of fluorescence in some cells was not due to the presence of inactive cells in the late stationary or death phase. The mean fluorescence intensities (expressed as RFU) were also obtained: 36.0 ± 8.7 , 66.5 ± 5.2 , 113.6 ± 9.9 , 161.9 ± 9.5 , and 205.7 ± 40.8 at 0, 2, 5, 10, and 20 h, respectively (Fig. S4), confirming a linear growth in fluorescence over the first 5 h of the assay.

Effects of thiols on As(III) uptake into cells. As a demonstration of the utility of this kinetic biosensor approach, we applied this method to determine the effects of organic molecules on rates of As(III) uptake into cells. Arsenic speciation analysis via high-performance liquid chromatography (HPLC)-ICP MS demonstrated that As was stable in its trivalent oxidation state in the presence of the model thiol compound glutathione (GSH) and the sulfur-rich Upper Mississippi natural organic matter (MNOM) (Fig. S5), even though the assay was performed aerobically. The terms $\Psi(t)$ and r, key factors in describing the As(III) uptake rate μ (equation 1), were calculated from fluorescence and OD_{600} measurements. Calculated $\Psi(t)$ and r are summarized in Fig. 4 and Table S1. The growth rate r did not change significantly in any experiment with GSH and oxidized glutathione (GSSG), indicating that the $\Psi(t)$ term by itself is sufficient to describe variations in As(III) uptake rates in the presence of GSH or GSSG. $\Psi(t)$ increased with greater As(III) concentrations, confirming that As(III) uptake rates depend on As(III) concentrations in the media. The quantity $\Psi(t)$ was also sensitive to the GSH/As(III) ratio, and for a given As(III) concentration, $\Psi(t)$ decreased as the molar GSH/As(III) ratios increased from 3:1 to 3,000:1 (Fig. 4a). The largest decreases in $\Psi(t)$ occurred with the highest fixed As(III) concentration, 3,200 nM, with statistically significant decreases, 30.0% \pm 4.4% and 34.7% \pm 5.2%, relative to the no-GHS (-GSH) control for the 300:1 and 3,000:1 GSH/As(III) ratios, respectively (Fig. 5a and Table S1). Note that the GSH/As ratio is fixed for each condition, so the higher As concentration does not imply a lower GSH/As(III) ratio. Importantly, GSSG at 300:1 and 3,000:1 GSSG/As(III) ratios and an As(III) concentration of 3,200 nM had no effect on $\Psi(t)$ (brown and blue

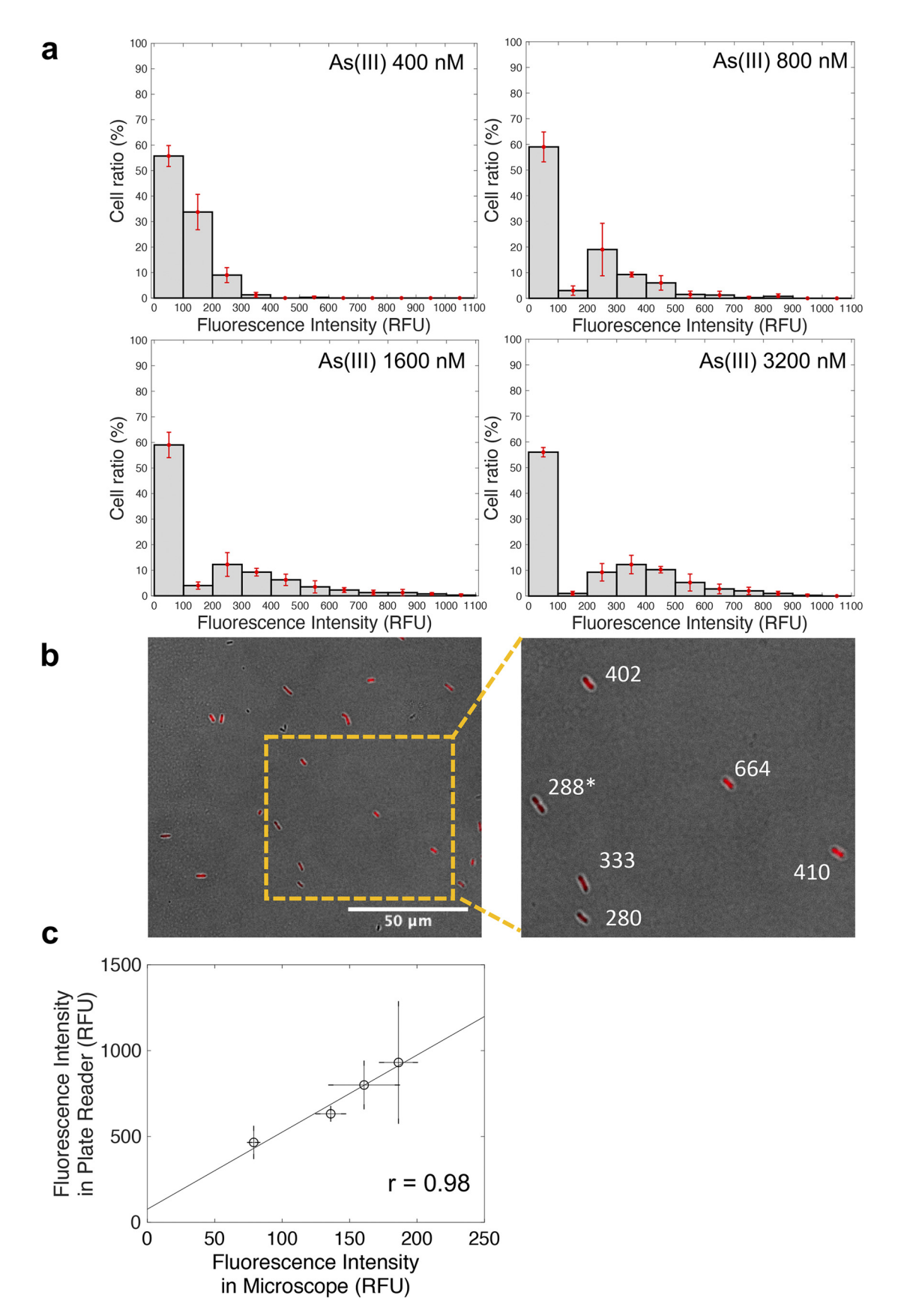


FIG 3 (a) Histograms of cell ratio (percentage of counted cells) versus fluorescence intensities measured by ImageJ software at four different As(III) concentrations. (b) Microscopic image of biosensor cells incubated with As(III) and quantification of fluorescence associated (Continued on next page)

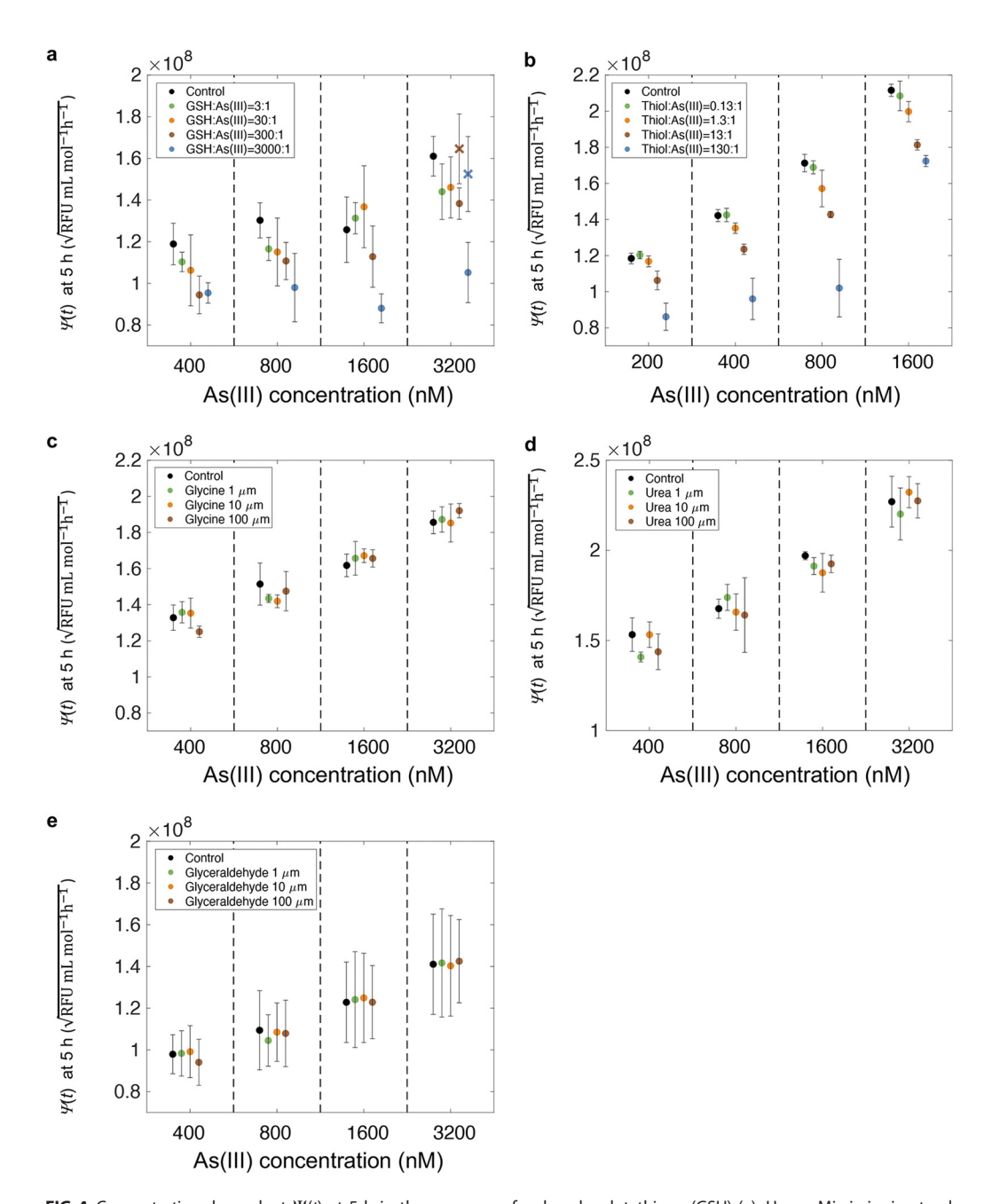


FIG 4 Concentration-dependent $\Psi(t)$ at 5 h in the presence of reduced L-glutathione (GSH) (a), Upper Mississippi natural organic matter (MNOM), expressed as the thiol concentration (b), glycine (c), urea (d), and L-glyceraldehyde (e). Oxidized L-glutathione at different ratios [brown cross, GSSG/As(III)) = 300:1; blue cross, GSSG/As(III)) = 3,000:1] was also tested with the GSH experiment. Fixed thiol/As(III) ratios were used for panels a and b, while fixed concentrations of organics were used for panels c to e. No inhibitor compounds were included in the control experiments. Each point represents the mean and standard deviation of four independently grown biological replicates. $\Psi(t)$ varied among different experiments due to variability in the biological reporting system.

crosses in Fig. 4a, respectively). GSSG is formed when GSH is oxidized and a disulfide bond is formed between the two S atoms. This finding therefore suggests that the reduced thiol moiety, and not some other functionality of the GSH molecule, was necessary for the observed inhibition. Glutamic acid and glycine, the amino acids that

FIG 3 Legend (Continued)

with individual cells. (c) Cross-analysis between mean fluorescence intensities measured with a plate reader and microscope. A bin of 0 to 100 RFU includes cells of fluorescence intensities less than the detection limit (<100 RFU) and was filtered out before calculating the mean microscope fluorescence intensity. Numbers in panel b (*) are measured values of each fluorescent cell by ImageJ software.

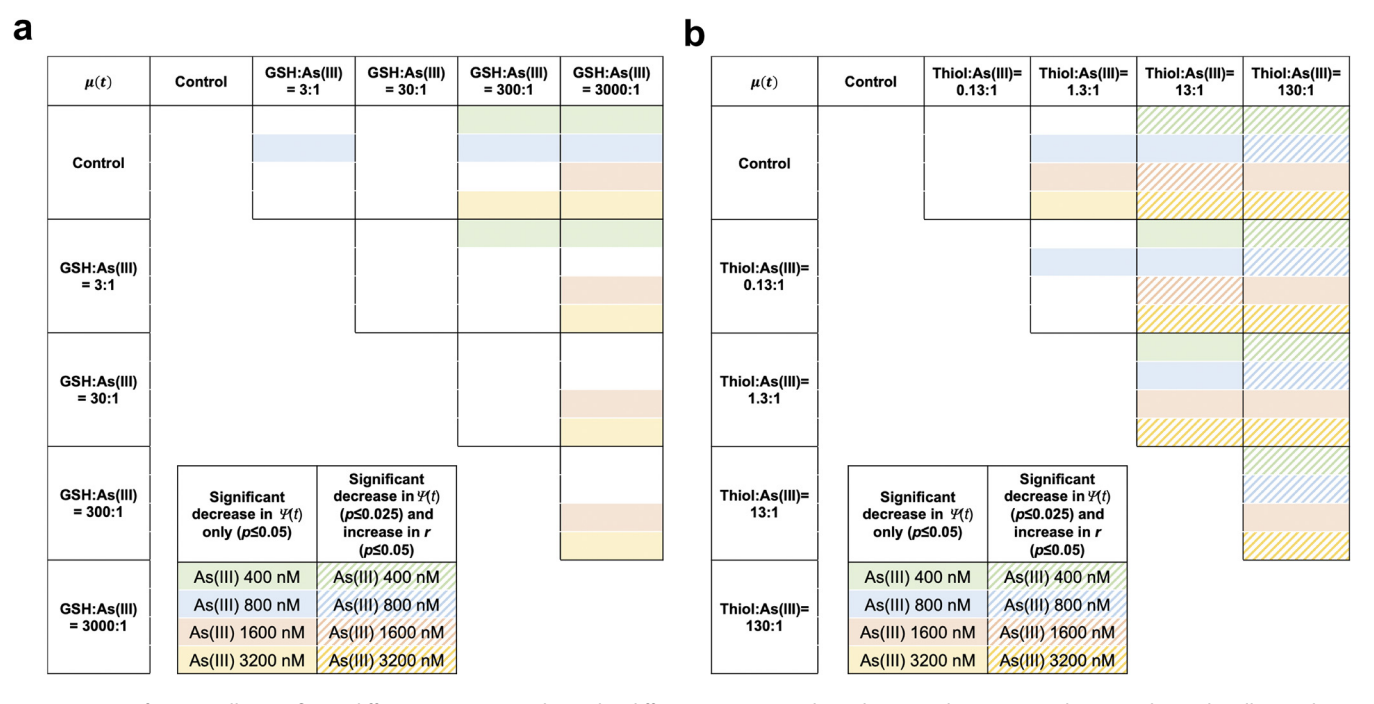


FIG 5 Matrix of statistically significant differences in $\Psi(t)$ and r under different experimental conditions with GSH (a) and MNOM (b). Each cell provides a pairwise comparison between a different thiol/As ratio. Solid color blocks represent treatments for which there is a significant decrease in $\Psi(t)$ only ($P \le 0.05$). Hatched color blocks represent significant decrease in $\Psi(t)$ and increase in r through multiple comparisons using Bonferroni-Holm method ($P \le 0.025$ for comparison of $\Psi(t)$; $P \le 0.05$ for comparison of P(t); $P \le 0.05$ for comparison of P(t) for P(t) fo

along with cysteine make up GSH, showed no inhibitory effects on As(III) uptake (Fig. 4c and Fig. S6, respectively), further demonstrating that the thiol group caused the observed inhibition.

The thiol binding site density in MNOM was determined to be 0.49 μ mol of thiol/ mg of C (Fig. S7), allowing the MNOM/As ratios to be expressed in terms of molar thiol/ As ratios (Fig. 4b). A systematic decrease in $\Psi(t)$ by MNOM was observed at thiol/As ratios of 13 and above, indicating inhibitory effects of MNOM on $\mu(t)$ (Fig. 4b and Table S2). MNOM exhibited a larger effect than GSH when normalized by thiol concentration, with statistically significant decreases in $\Psi(t)$ of 27.3% \pm 2.5%, 32.4% \pm 3.9%, 40.4% \pm 6.4%, and 76.7% \pm 14.2% at the 130:1 ratio with initial As(III) concentrations of 200, 400, 800, and 1,600 nM, respectively, relative to the control (Fig. 4b and Table S2). MNOM had a negligible effect on r at the ratios of 0.13:1 and 1.3:1, but r increased at higher thiol/As(III) ratios that corresponded to greater dissolved organic carbon (DOC) concentrations. Following equation 1, increases in r imply additional decreases in $\mu(t)$ beyond changes observed in $\Psi(t)$. Figure 5 shows pairwise comparisons of statistically significant decreases in $\Psi(t)$ and increases in r between different thiol/As ratios. This provides a semiquantitative comparison between effects of different thiol/As(III) ratios on As(III) uptake, since decreasing $\Psi(t)$ and increasing r both imply inhibited uptake kinetics. For MNOM, decreases in $\Psi(t)$ correspond to either increases in r or no change in r (i.e., there is no case where r decreases) (Fig. 5b), so MNOM has an unambiguous inhibitory effect on As(III) uptake.

While direct comparison between MNOM and GSH is hindered by the fact that the thiol/As ratios are somewhat different, the significant effect on $\Psi(t)$ at MNOM-thiol/As ratios as low as 13:1, coupled with an extent of inhibition at a MNOM-thiol/As ratio of 130:1 comparable to that at a GSH:As ratio of 3,000:1, indicates that MNOM is more effective at inhibiting As uptake than GSH. An additional feature of the MNOM beyond the thiol ligands may thus play a role in the observed inhibition.

The effects of MNOM on inhibiting As(III) uptake were confirmed with single-cell fluorescence microscopy, where measurements with 400 nM As(III) in the presence of 83.2 mg of C/L of MNOM showed that fluorescence intensity was decreased by 45.8%

Downloaded from https://journals.asm.org/journal/aem on 12 September 2022 by 128.84.126.165.

compared to that for a control without MNOM (Fig. S8). The fact that this effect was seen in microscopic imaging, in which only a thin layer of cell suspension was placed onto a slide, indicates that the decrease in measured fluorescence was not due to fluorescence absorption by DOM. This conclusion was also supported by a follow-up analysis in which the biosensor was exposed to 3,200 nM As for 20 h without MNOM before being diluted 1:1 in 800 mg of C/L of MNOM for plate reader fluorescence measurement (Fig. S9). Measured endpoint fluorescence of the MNOM-diluted biosensor (859.3 \pm 37.6 RFU) was similar to the sum of that from biosensor diluted 1:1 in a 0.1 M NaCl solution (438.8 \pm 13.8 RFU) and background autofluorescence from MNOM itself (441.0 \pm 7.1 RFU). Note that in our kinetic assay, autofluorescence of the MNOM is background subtracted and has been shown not to change as a function of time (Fig. S10). We also tested whether there were pH-dependent effects of thiols on uptake rates by performing experiments at pHs 6.8 and 7.8, and we found that changing pH did not significantly impact the results (Table S3). This was expected since neither As (III) $(pK_a = 9.2)$ nor thiols $(pK_a = 9.7)$ (Table S4) experience a change in speciation across this pH range.

Effects of small organic molecules on As(III) uptake. The effects of glycine, urea, and glyceraldehyde on $\Psi(t)$ and r were repeatedly tested to evaluate potential competition between neutral, small organic molecules and As(III) for uptake through GlpF channels (26, 27). None of the organic molecules exhibited significant inhibitory effects on $\Psi(t)$, and r was only increased in two cases of As(III) in the presence of glycine (Fig. 4c to e and Table S5). Because r increased, we cannot completely rule out an inhibitory effect of glycine on As(III) uptake, but the lack of any impact on $\Psi(t)$ suggests that any change would have been relatively small.

Comparing the kinetics-based approach with fluorescence endpoint analysis. Biosensor studies have traditionally used endpoint fluorescence measurements to determine differences in As bioavailability (57, 58). In this study, we compared the results of OD_{600} -normalized endpoint fluorescence measurements (F_{RFU} [5 h]/OD₆₀₀) with our kinetics-based analysis [$\Psi(t)$ at 5 h] of the fluorescence time series from a representative experiment with As(III) and MNOM. We did this to evaluate the sensitivities of different approaches for interpreting biosensor fluorescence data and effects of inhibitory substances on As(III) uptake. Both approaches showed increases in As bioavailability as the initial As(III) concentration increased and diminished As bioavailability as the thiol/As ratio increased (Fig. 6). The two methods were similarly effective at distinguishing statistically significant differences in As uptake at different thiol/As ratios. This finding serves to validate the use of endpoint fluorescence measurements, since the endpoint measurements are for the most part comparable with our results which were derived from a rigorous mathematical framework for interpreting biosensor fluorescence in the context of the negative-feedback ArsR-based bioreporter system.

DISCUSSION

The As biosensor literature is currently divided between experimental investigations that correlate endpoint fluorescence measurements to As uptake and those that use synthetic biology kinetic modeling of the ArsR negative-feedback circuit. The latter approaches account explicitly for the detailed mechanism of translation and transcription, but rely on a large number of fit parameters that can limit the practical application of these models. Here, we provide a middle ground with a model framework for using frequently measured variables ($F_{\rm RFU}$ and r) along with a small number of parameters (Table 1) to enable analysis of As uptake kinetics and how they are affected by DOM quantity and quality. A limitation to our approach is that since we do not know the value of γ (the RFU per molar concentration of mCherry protein), the expression for As(III) uptake μ (equation 1) cannot be fully quantified. Instead, we use relative changes in $\Psi(t)$ and r to determine semiquantitative changes in μ , assuming that γ is constant. This approach provides unambiguous, novel evidence for inhibited cellular uptake of As(III) in the presence of GSH and MNOM. Future work to quantify γ could enable a fully quantitative evaluation of As(III) uptake kinetics using this framework.

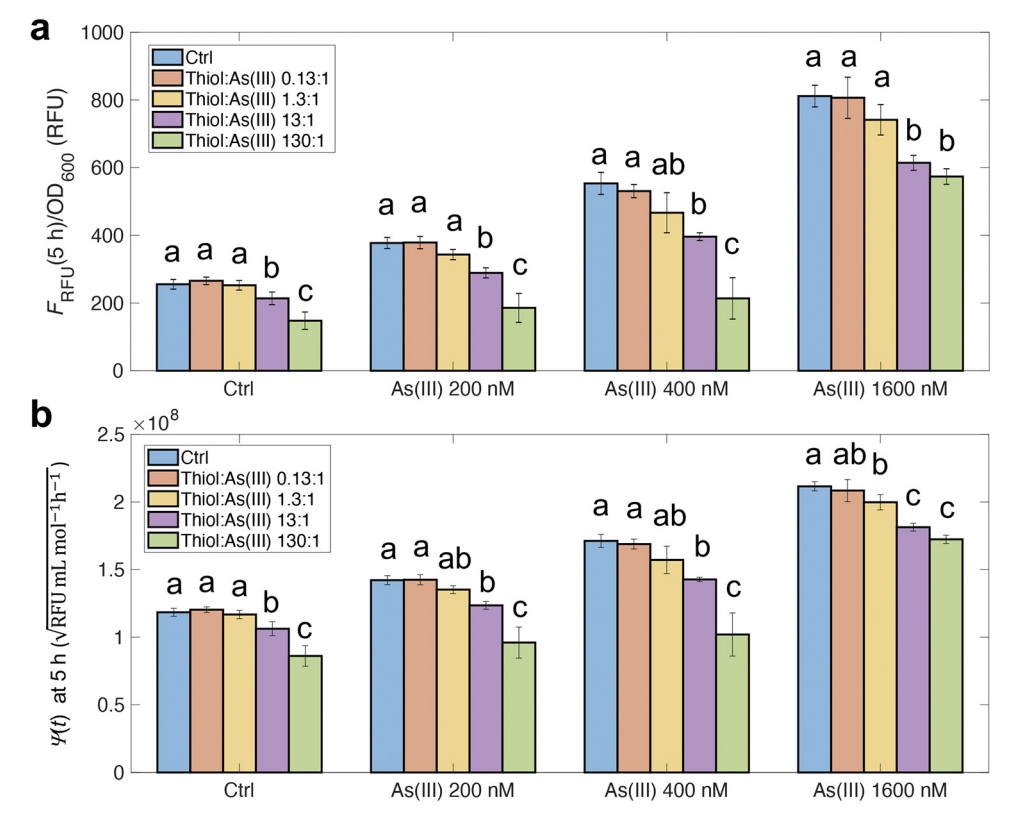


FIG 6 Bar graphs of end points at 5 h from biosensor experiments with different ratios of MNOM to As(III) (a) and $\Psi(t)$ at 5 h from the same experiments (b). The key is expressed as the molar ratio of MNOM-associated thiols to As. A letter over each bar indicates significant difference ($P \le 0.05$) within a group of different MNOM/ As ratios at the same As(III) concentration.

A potential impediment to performing the biosensor assay in the presence of DOM in 96-well plates is that fluorescence emitted by cells could be attenuated by DOM before being detected by the plate reader. Fluorescence microscopy of As(III) in the presence of MNOM, involving a very thin layer of medium, was consistent with outcomes from the plate reader (Fig. S8), indicating that attenuation of biosensor fluorescence did not significantly affect the data. This conclusion was further supported by testing the fluorescence of the biosensor exposed to As(III) for 20 h before being added to MNOM and noting that there was negligible change in the measured fluorescence once MNOM autofluorescence was accounted for (Fig. S9).

Interestingly, microscopy revealed that roughly 60% of the cells had fluorescence intensities below the limit of quantification (LOQ, <100 RFU), and there was a broad distribution in fluorescence intensities from cells in the same assay. The distribution in fluorescence intensities may be due to the highly variable copy number of pUCP19, mCherry-bearing plasmids in E. coli cells (59). From the time series microscopy of the biosensor incubated with As(III), the ratios of cells with fluorescence less than the LOQ were similar (50.8 to 58.0%) from the exponential phase to stationary phase (Fig. S3). Note that all cells were grown with ampicillin, and microscopy showed that all cells had similar morphologies, so contamination of the culture is highly unlikely. The presence of a considerable fraction of cells with fluorescence less than the LOQ suggests that the arsRBC operon may display bistability. Bistable responses have been characterized for several inducible promoters, for example, for the lac operon in E. coli and for the galactose gene regulatory network in Saccharomyces cerevisiae, but to the best of our knowledge, they have not been previously observed for the arsRBC operon. Several mechanisms that can cause bistable regulation have been identified (60), such as positive-autoregulation and negative-feedback loops, and future research will be

Downloaded from https://journals.asm.org/journal/aem on 12 September 2022 by 128.84.126.165.

devoted to identifying the specific mechanism responsible for the observed bistability of ArsR-regulated promoter *arsRp* expression.

To further explore the phenomenon of cells with fluorescence less than the LOQ, cells from a biosensor overnight culture were grown on an LB agar plate containing 3,200 nM As and 120 μ g/mL of ampicillin and examined by microscopy. All of the colonies exhibited fluorescence (Fig. S11a). However, when a colony was streaked onto a glass slide, a significant fraction of cells had fluorescence less than the LOQ (Fig. S11b). This indicates that the subpopulation with zero to minimal fluorescence evolved from an ancestor with fluorescence capabilities, which is corroborated by the absence of clonal nonfluorescent and fluorescent sectors that would be observed in the colonies if the lack of fluorescence was transmitted vertically between cells (61). Plasmids were extracted from colonies on the LB agar plate with high (>3,000 RFU) and low (<1,500 RFU) fluorescence and sequenced using full-length plasmid sequencing (www .plasmidsaurus.com), a technique that allows detection of cells harboring multiple, different plasmids. All plasmids extracted from colonies had the same length consistent with the sum of pUCP19 and the construct containing arsR and mCherry (Fig. S12), ruling out the possibility that a conspicuous subpopulation of cells had lost the mCherry gene or other components of the engineered plasmid. Additionally, because all experiments were performed by adding ampicillin to the medium, there was less chance of loss of the plasmid at cell division. The presence of cells with fluorescence less than the LOQ therefore seems to be phenotypic rather than genotypic, and the underlying mechanism is currently unknown. While the observations of cells with minimal fluorescence is interesting, it does not negatively impact the quantitative interpretation of fluorescence data since the mean of the fluorescence distribution increased with increasing As(III) concentrations and was strongly correlated with total fluorescence measured with the plate reader (Fig. 3).

A key finding of this study is that thiol-containing compounds significantly decreased As(III) uptake rates (Fig. 4a and b). GSH and the thiol-containing environmental isolate MNOM significantly inhibited As uptake, while oxidized glutathione (GSSG), glutamic acid, and glycine had no systematic effect on uptake, indicating that the thiol moiety in GSH and not another feature of the GSH molecule caused the inhibition (Fig. 4 and Fig. S6). Similarly, the fact that LMW, neutral organic molecules did not inhibit uptake suggests that small neutral molecules which could be present in the MNOM environmental isolate were not the drivers of inhibited uptake.

Arsenite is known to complex with model LMW thiols like GSH and dithiothreitol (44) and with thiol-enriched humic acids (42). Phytochelatins bind As(III) through thiol moieties (62), and more recently, organosulfur groups in peat NOM have been shown to sequester As(III) (43). Our group recently showed that the organic S content of DOM was a good predictor of As(III)-DOM complexation, and this was hypothesized to be related to higher thiol site densities in S-rich DOM like MNOM (63). Here, we suggest that diminished As uptake in the presence of thiol ligands is due to formation of aqueous As(III)-thiol complexes with lower bioavailability than unbound As(III). Greater inhibition at higher DOM-thiol/As ratios is similar to well-known findings for mercury (64). Decreased uptake of thiol-bound As through GIpF channels will likely be impacted by the larger size of the complex than for unbound As(III), as well as the charge of the complex. The As(GS) $_3$ complex, with a net charge of -3, is thought to be the most stable complex as long as GSH is not limiting (44). It is highly probable that a net negative charge will be conferred to the As-thiol complexes formed with MNOM because most aquatic organic matter has a net negative charge at circumneutral pH (65). Because GlpF is permeable only to uncharged species, the significant decrease in As uptake in the presence of GSH and MNOM may be partly attributed to the exclusion of charged solutes by GlpF (66).

As(III) uptake was significantly inhibited by GSH at molar thiol/As(III) ratios at 3,000:1 (Fig. 5a and Table S1), with the differences most apparent at As concentrations of 1,600 nM and 3,200 nM. These findings are broadly consistent with equilibrium

August 2022 Volume 88 Issue 16

Downloaded from https://journals.asm.org/journal/aem on 12 September 2022 by 128.84.126.165

modeling of As(III)-GSH complexation (Fig. S13), using stability constants provided in the work of Spuches et al. (44). The modeling shows that significant As(III)-GSH complexation is expected at the 3,000:1 ratio and not the 300:1 ratio, consistent with our experimental biosensor findings. The modeling also shows that roughly 90% of As(III) would be bound to GSH at a GSH/As(III) ratio of 3,000:1 when the As(III) $_{\rm tot}$ is 3,200 nM, leaving approximately a 320 nM concentration of the As(III) unbound. Biosensor data show that the $\Psi(t)$ term for this condition is similar to the $\Psi(t)$ term for the -GSH control with 400 nM As(III), all of which would have been unbound. This comparison shows good agreement between the semiquantitative interpretation of biosensor data for inhibited uptake and the As(III)-GSH complexation modeling for fraction of unbound, and presumably bioavailable, As(III).

MNOM caused significant inhibition starting at lower thiol/As ratios of 13:1 and above (Fig. 5b). The reasons for inhibition at this relatively low thiol/As ratio are not clear, but findings by Abu-Ali et al. (63) of significant As(III)-MNOM complexation at thiol/As ratios as low as 37:1 suggest that thiols in MNOM may have a higher affinity for As(III) than GSH. The literature shows a wide range of stability constants for complexation between model thiol compounds and As(III) (44). Dissolved thiol concentrations can reach 30 μ M in DOM-rich waters (67, 68), leading to thiol/As ratios with a characteristic range of ~10:1 to 40:1 based on the range of As concentrations typically observed in soil-water systems (28, 69). In this study, MNOM-thiol concentrations of 10.0 or 20.0 μ M (equivalent to 20.4 and 40.8 mg of C/L) were associated with substantial inhibition of uptake of 800 or 1,600 nM As(III), indicating that DOM may significantly diminish As(III) bioavailability at environmentally relevant DOM/As ratios. We acknowledge that the thiol binding site density for MNOM of 0.49 μ mol of thiol/mg of C, determined via monobromo(trimethylammonio)-bimane (qBBr) fluorescence spectroscopy (67), is relatively high compared to estimates with other aquatic DOM (64, 70-72). The estimated thiol density represents roughly 30% of the total organic S content of the MNOM, based on the S/C ratio provided by the International Humic Substances Society (IHSS) of 1.64 μ mol of S/mg of C. This thiol fraction is similar to, though slightly higher than, the range of thiol percentages reported for aquatic organic matter by Skyllberg et al. (73).

Our results with LMW neutral molecules (Fig. 4c to e) showed that there was no systematic evidence of an important role for competitive inhibition of uptake through GlpF channels. This is consistent with knowledge of GlpF as a passive transporter (26, 74, 75), with prior studies of As(III) uptake in the presence of antimonite (p $K_a = 11.8$) also showing a lack of competitive interactions (19). Importantly, organic matter may also lead to decreased uptake of As(III) through a catabolite repression mechanism, in which the GlpF uptake site density is decreased due to downregulation of glpF in the presence of high levels of labile carbon substrates. In our study, MNOM was shown to inhibit As(III) uptake to a greater extent than GSH when normalized by the thiol site density. While this may be due in part to differences in binding affinities, there is also a possible role for a separate inhibitory mechanism like catabolite repression. OD₆₀₀ was higher in the MNOM experiment than for the control (Table S2), indicating the likely presence of labile carbon in the MNOM pool. GSH did not affect OD_{600} , suggesting that catabolite repression did not contribute to the inhibited uptake observed in the presence of GSH (Table S1) (76). It is also possible that the Fe content of MNOM of 1.31 μ g of Fe/mg of C (Table S6) may lead to formation of ternary DOM-Fe-As(III) complexes as another mechanism for DOM-As(III) complexation (77). For MNOM, the potential for catabolite repression and ternary complexation in addition to complexation via direct binding between thiols and As highlights the multiple mechanisms through which complex DOM pools may inhibit microbial As(III) uptake.

In this study, *E. coli* was used as a model organism to examine bacterial As(III) uptake, and it is common for physiological insights gained from *E. coli* to be generalized to other bacteria (78, 79). While we acknowledge that the aerobic conditions of the assay are not ideal for characterizing dynamics of As(III), this was required for growth of the biosensor construct, and similar experimental conditions are frequently

described in the biosensor literature (50, 54, 56). We confirmed with HPLC-ICP MS analysis that As was stable in its trivalent oxidation state throughout the assay (Fig. S14). New insights from this work on factors regulating microbial uptake of As may thus have generalizable implications for management of arsenic-contaminated sites. For example, reduction of As(V) to As(III) via intracellular ArsC may affect As adsorption to soil minerals or engineered adsorbents (80), and production of methylated As species via intracellular ArsM can affect ratios of methylated to inorganic As in rice grains, impacting toxicity (81). Changes to As speciation affecting uptake through bacterial GIpF could also impact phytoremediation efforts, since the aquaporin channels through which plants take up As(III) are in the same protein family as GIpF (82–84).

Conclusions. We developed a new mathematical framework for determining kinetics of cellular uptake of As using biosensor fluorescence data, and we applied this method to show that thiol-containing organic molecules, including an S-rich environmental organic matter isolate, significantly inhibit microbial As(III) uptake at environmentally relevant DOM/As ratios. LMW neutral molecules did not inhibit As(III) uptake. The inhibition of As(III) uptake in the presence of thiol ligands is hypothesized to be due to formation of aqueous As-thiol complexes with net negative charges and/or molecular weights that prevent their transport across cell membranes. In more complex DOM pools containing labile C, catabolite repression may also impact As(III) uptake, and research is under way to disentangle inhibitory mechanisms involving restricted transport due to As(III)-DOM complexation versus effects on the GlpF uptake site density due to catabolite repression. These biosensor results provide novel insights into As (III)-DOM interactions in the environment and how these interactions may regulate microbial As(III) uptake and downstream As biotransformation processes.

MATERIALS AND METHODS

Mathematical model development. Our phenomenological model is based on the observation that fluorescence intensities increased linearly over the first 5 h of the assay at all As(III) concentrations investigated (Fig. 2 and Fig. S2). It was further supported by the fact that the half-life of mCherry protein is on the order of 24 h (85, 86), so the effects of mCherry decay during the initial 5 h can be neglected. Expression of the *arsR* gene occurs when the first ArsR binding site (ABS) on the plasmid is left unoccupied, due to binding between As(III) and ArsR in the cytoplasm (Fig. 1). Accounting for population growth and DNA replication, the total number of operators ABS_T in the population satisfies the equation

$$\frac{dABS_{T}}{dt} = rABS_{T} = rABS_{c}N(t) = 2rP_{N}N(t)$$
 (2)

where r and N(t) are the cells' growth rate (per hour) and the cell number at time t (moles per milliliter), respectively. N(t) was determined from OD_{600} measurements. Measured OD_{600} was converted to cell number per volume and biomass per volume through a calibration curve obtained using a serial dilution assay (Fig. S15) (87). ABS_c is the average number of ABSs per cell (moles per mole), which is approximately twice the average plasmid copy numbers per cell (P_{Ni} moles per mole) since there are two ABSs per plasmid.

Since there are one ABS upstream and one downstream of *arsR*, expression of the *mCherry* gene occurs only when both ABSs on the plasmid are unbound (Fig. 1). We can estimate the probability that a given operator is unbound as $p = \text{ABS}_u/\text{ABS}_{Tr}$ where ABS_u is the number of operators unbound by ArsR. The translation/transcription rate of *arsR* is then assumed to be proportional to half the number of unbound operators, as the other half of ArsR may bind to the downstream operator, thus

$$\frac{dArsR_{T}}{dt} = \beta P_{N} pN(t) = \frac{ABS_{T}}{2} p = \frac{\beta}{2} ABS_{u}$$
 (3)

where ArsR_{r} , β , and P_N are the total number of ArsR protein (moles per milliliter), the rate of transcription/translation of arsR per ars promoter (per hour), and the average number of plasmids per cell (moles per mole), respectively. $\operatorname{ABS}_{r}/2$ is the number of operator pairs. We neglect the chromosomal arsR gene because arsR copies in plasmids are assumed to outnumber those in chromosomal genes. Likewise, the translation/transcription rate of the $\operatorname{mCherry}$ gene is assumed to be proportional to the number of unbound pairs of operators, that is,

$$\frac{dmCherry}{dt} = \beta P_N N(t) p^2 = \beta \frac{ABS_T}{2} p^2 = \frac{\beta}{2} \frac{ABS_u^2}{ABS_T}$$
 (4)

where β is here the rate of transcription/translation of *mCherry* per *ars* promoter (per hour). The translation rate of *arsR* and *mCherry* could be different (54), but β values of *arsR* and *mCherry* were assumed to be the similar, in the range of 43.2 to 50.4 h⁻¹ (Table 1) for development of a simpler mathematical

framework. The experimental observation that the total fluorescence intensities (proportional to mCherry concentrations) showed a linear increase with time implies that

$$\frac{dmCherry}{dt} = \frac{\beta}{2} \frac{ABS_{u}^{2}}{ABS_{T}} \equiv \alpha = constant$$
 (5)

It follows that

$$ABS_{u} = \sqrt{\frac{2 \alpha}{\beta} ABS_{T}}$$
 (6)

Differentiating equation 5 with respect to time gives

$$\frac{d}{dt}\frac{ABS_{u}^{2}}{ABS_{T}} = 2\frac{ABS_{u}}{ABS_{T}}\frac{dABS_{u}}{dt} - \frac{ABS_{u}^{2}}{ABS_{T}^{2}}\frac{dABS_{T}}{dt} = 0$$
(7)

Rearranging and substituting equation 2 gives

$$2\frac{dABS_{u}}{dt} = \frac{ABS_{u}}{ABS_{T}}rABS_{T} = rABS_{u}$$
(8)

The repressor ArsR has a high binding affinity for As(III), as even concentrations on the order of 10^{-15} M can derepress the operator and express downstream genes (53, 88). Thus, we assume that As(III) that enters the cell immediately binds an ArsR, which could have been either bound or unbound to the operator. To be consistent with the rates described above, the rate of increase of bound operators ($dABS_b/dt$) must be related to the difference between the rate of ArsR translated and the net rate of As(III) uptake into cells:

$$\frac{dABS_b}{dt} = \frac{dABS_T}{dt} - \frac{dABS_u}{dt} = \frac{1}{2} \left(\frac{dArsR_T}{dt} - \frac{dAs_c}{dt} \right)$$
(9)

where the factor 1/2 is from the assumption that the repression of one ABS requires an ArsR dimer which dissociates and derepresses the operator when the dimer binds to two As(III) molecules. The assumption is based on previous reports that ArsR needs to be dimerized for its binding to ABS (89) and an ArsR dimer has two As(III) binding sites which have same affinities to As(III) (54, 90). We derived the net uptake of As(III) per cell at time t [μ (t); moles per mole per hour] by combining equations 2, 3, and 8 as follows:

$$\mu(t)N(t) \; \equiv \; \frac{d {\rm As_c}}{dt} = \; \sqrt{\frac{dm {\rm Cherry}}{dt}} \, \beta \, P_N \, N(t) \; + \; 2r \sqrt{\frac{dm {\rm Cherry}}{dt}} \, \frac{1}{\beta} \, P_N \, N(t) \; - \; 4r \, P_N \, N(t) \; \qquad (10)$$

See the supplemental material for additional details on how the equations were combined to give equation 10. Since *mCherry* is the total number of moles of mCherry proteins, equation 10 can be expressed as

$$\mu(t) = \sqrt{\frac{1}{N(t)}} \frac{dF_{\text{RFU}}}{dt} \sqrt{\frac{P_N}{\gamma}} \left(\sqrt{\beta} + \frac{2r}{\sqrt{\beta}}\right) - 4r P_N$$
 (11)

using $F_{RELI} = \gamma mCherry$ where γ is RFU per molar concentration of mCherry protein.

The parameter r was determined using experimentally measured values (0.082 to 0.127 h⁻¹ [Table 1]), and the parameter β was obtained using translation and transcription rate estimates (Table 1) from the work of Berset et al. (54) (43.2 to 50.4 h⁻¹ [Table 1]). Using these values, it can be inferred that $\sqrt{\beta}$ is significantly larger than $\frac{2r}{\sqrt{\beta}}$; therefore,

$$\mu(t) \equiv \sqrt{\frac{1}{N(t)}} \frac{dF_{\text{RFU}}}{dt} \sqrt{\frac{P_N}{\gamma}} \sqrt{\beta} - 4r P_N = \Psi(t) \sqrt{\frac{P_N}{\gamma}} \sqrt{\beta} - 4r P_N$$
 (12)

where $\Psi(t)$ is introduced as a lumped parameter for $\sqrt{\frac{1}{N(t)}\frac{dF_{BFU}}{dt}}$ for the convenience of the readers.

Sensitivity analysis. A sensitivity analysis was performed to compare the sensitivity of the net As(III) uptake rate $\mu(t)$ to changes in $\Psi(t)$ or r. For each analysis, $\Psi(t)$ or r was increased by 10% and the change of $\mu(t)$ was calculated to obtain the relative sensitivity function (RSF), that is,

RSF of
$$\Psi (t) = \frac{\Delta \mu(t)}{\mu(t)} \times \frac{\Psi(t)}{\Delta \Psi(t)}$$
 (13)

RSF of
$$r = \frac{\Delta\mu(t)}{\mu(t)} \times \frac{r}{\Delta r}$$
 (14)

RSFs were calculated and shown in Fig. S16 with the assumption that the constant γ is in the range of 10¹² to 10¹⁶ RFU mL mol⁻¹, determined by dividing measured fluorescence intensities of biosensor (0

Downloaded from https://journals.asm.org/journal/aem on 12 September 2022 by 128.84.126.165

to 1,000 RFU [Table 1]) by the cell number (0.43 \times 10⁻¹⁵ to 1.29 \times 10⁻¹⁵ mol mL⁻¹ [Table 1]) and the previously reported translation rate of the reporter gene (662.4 h⁻¹ [54]) and duration of experiments (5 to 20 h). This sensitivity analysis demonstrated that $\mu(t)$ is at least an order of magnitude more sensitive to $\Psi(t)$ than r in the assumed range (Fig. S16).

Biosensor growth media and arsenic uptake assay. A whole-cell *E. coli* biosensor was used to quantify uptake kinetics of As(III) into cells (91). The plasmid pUCP19 shuttle vector engineered to contain As-sensing and reporting genes (arsR and mCherry) was transformed into *E. coli* NEB 10-beta (New England Biolabs) (Fig. 1), a derivative of DH10B. Notably, the reporter construct was designed to contain two ArsR binding sites upstream of the arsR and mCherry genes to reduce the background expression of mCherry. Details on the construction of the whole-cell *E. coli* biosensor are available in reference 15. For each experiment, the *E. coli* biosensor was thawed from a cryostock and plated onto an LB plate containing 120 μ g/mL of ampicillin. The LB plate was incubated overnight at 37°C. Experiments were performed with biological quadruplicates, with four independent colonies inoculated into different autoclaved narrow-mouthed Pyrex 125-mL flasks containing 100 mL of growth medium with 120 μ g/mL of ampicillin at pH 7.8 (15). A complete description of the growth media is available in the supplemental material. Culture flasks were incubated on an orbital shaker at 37°C and 200 rpm.

As(III) uptake kinetics were determined by exposing the biosensor to As(III) over a concentration range of 200 to 3,200 nM and measuring fluorescence intensities at 20-min intervals for 20 h at 37°C. Growth media with 120 μ g/mL of ampicillin, As(III), and inhibitory compounds (e.g., thiols; small organic molecules; summarized in Table S4) were preincubated for 2 to 3 h inside an anaerobic chamber (Coy Laboratory Products), and then 400 μ L of the precultured biosensor was added. A total of 200 μ L was plated in each well of a Corning 96-well plate for fluorescence measurements. Each condition was tested with four biological replicates. Controls without As(III), without inhibitory compounds, or without cells were measured in parallel.

Fluorescence intensities and OD_{600} s were measured with an Infinite 200 fluorescence plate reader (Tecan, Research Triangle Park, NC) or with a Synergy H1 hybrid reader (BioTek, Winooski, VT). The fluorescence intensity from the time zero sample was background subtracted from subsequent samples to account for DOM autofluorescence or the effects of photon scattering by DOM or other solutes. The excitation wavelength was 560 nm, and fluorescence was measured at 620 nm. In order to ensure that As (III) did not oxidize to As(V) during biosensor assays, filtered samples of the assay with organic molecules were analyzed for arsenic speciation using HPLC-ICP MS for the full duration of the experiments (Fig. S5). For all experiments, significant differences between experimental conditions were assessed using oneway analysis of variance (ANOVA) with Tukey's post hoc test using R (92), with differences considered to be significant when the P value was \leq 0.05.

Validation of fluorescence data from plate reader with microscopy. Fluorescence microscopy was performed to confirm that fluorescence readings in the plate reader were consistent with fluorescence measured via microscope at the single-cell level (Fig. S17d) and to account for potential attenuation of biosensor fluorescence that could be caused by DOM in the plate reader. The arsenic uptake assay in biological replicates was prepared with four different As concentrations (400, 800, 1,600, and 3,200 nM), and the fluorescence was measured with a plate reader over 20 h. After the measurements, 5 μ L was withdrawn from each well of a 96-well plate for fluorescence microscopy analysis and placed on a microscope slide. Fluorescence imaging was performed on a Zeiss Axio Scope A1 fluorescence microscope (Carl Zeiss, Oberkochen, Germany) with filter set 95 (excitation DBP 475/20 + 585/25; emission DBP 518-25 + 625-30) and objective EC Plan-Neofluar 40×/0.75 Ph2 M27. For each As concentration, 100 individual cells were randomly selected in the recorded images and their fluorescence intensity was quantified using ImageJ/Fiji (Fig. 3b). Time series measurements were also performed with the biosensor strain incubated with 3,200 nM As(III) for 20 h. Four replicates were prepared, and at each time point (0, 2, 5, 10, and 20 h), 5 μ L of each was withdrawn for fluorescence microscopy analysis. In order to investigate the distribution of cell fluorescence, fluorescence imaging was performed with colonies grown with 3,200 nM As(III) and 120 µg/mL of ampicillin on LB plates using an EC Plan-Neofluar 10×/0.3 Ph1 M27 objective. Among all colonies, a single fluorescent colony was picked randomly and placed on a microscope slide for fluorescence microscopy analysis. Information about the distribution of fluorescence of biosensor cells is detailed in the supplemental material.

Effects of thiols on As(III) uptake. Reduced L-glutathione (GSH; Alfa Aesar) was selected as a model thiol compound to test the effects of thiols on cellular uptake of As(III). GSH was added at molar GSH/As (III) ratios of 3:1, 30:1, 300:1, and 3,000:1. The stoichiometric ratios are based on observed 3:1 coordination between GSH and As(III) (44) and were selected to span an environmentally relevant range of thiol/ As ratios, Oxidized L-glutathione (GSSG: Alfa Aesar) was tested to evaluate whether the oxidation of thiols to form disulfides affects the interaction between organosulfur compounds and As(III). Experiments were also performed with glutamic acid and glycine to evaluate the effects of the amino acids that, along with cysteine, make up GSH. Upper Mississippi natural organic matter (MNOM; code 1R110N; International Humic Substances Society [IHSS], St. Paul, MN) was selected to test the effects of an aquatic NOM on As(III) uptake. MNOM has a relatively high sulfur content (93) and is therefore more likely to have a higher density of thiol binding sites than other reference materials. The MNOM experiments were performed with MNOM/As(III) ratios of 0.27, 2.7, 27, and 270 mg of C/µmol of As(III). These ratios were chosen for their environmental relevance to rice paddy environments with moderate As contamination (69). In order to assess the autofluorescence of MNOM and the E. coli biosensor, both a plate reader and microscopy were used to assess fluorescence of E. coli only and that of 83.2 mg of C/L of MNOM and 400 nM As(III) without cells. The potential effect of MNOM on attenuating measurements of biosensor fluorescence was assessed as follows. Biosensors with 3,200 nM As(III) were grown for 20 h, and at the endpoint, twice diluted with 800 mg of C/L of MNOM or 0.1 M NaCl. A total of 800 mg of C/L of MNOM was also twice diluted with NaCl (0.1 M) solution, and fluorescence intensities were compared.

August 2022 Volume 88 Issue 16

Effects of organics on As(III) uptake at different pHs. The effects of organics, including GSH, GSSG, and MNOM, on As(III) uptake were evaluated at pHs 6.8 and 7.8 to examine if different pHs cause differences in DOM-As(III) complexation and result in different As(III) uptakes. Both growth media and working media were adjusted to pHs 6.8 and 7.8 for each condition before adding inoculum, and they were exposed to As(III) and organics and incubated for 20 h in four replicates. As(III) and organics were mixed and incubated on the rotator overnight prior to the exposure to cells, in order to ensure the formation of As(III)-thiol complexes.

Effects of small organic molecules on As(III) uptake. The effects of urea, glycine, and pt-glyceraldehyde on As(III) uptake were tested because these molecules are taken up into cells through GlpF transporters (19, 21, 26). These organic compounds were purchased from VWR and were prepared in fresh stock solutions and amended to each array at 1, 10, or 100 μ M.

Chemical analyses. Arsenic was measured at m/z = 75 using an Agilent 7800 ICP MS with a helium collision cell and with rhodium as an in-line internal standard. Quality control was performed by periodic measurement of standards, blanks, and repeat samples. Arsenic speciation analysis was performed using HPLC-ICP MS (Agilent 1260 Infinity HPLC with an Agilent 7800 ICP MS), with a PRP-X100 anion exchange column (94, 95). Details of the speciation analysis are in the supplemental material. The dissolved organic carbon concentration of the MNOM solution was measured using a Shimadzu TOC-L analyzer (non-purgeable organic carbon [NPOC] method). The thiol concentration in MNOM was quantified using a monobromo(trimethylammonio)-bimane (qBBr) fluorescence spectroscopy method described by Joe-Wong et al. (67).

Data availability. The nucleotide sequence of the reporter construct of biosensor used in the study is available in the supplemental material. Code used in the interpretation of biosensor fluorescence data, along with a sample data set, is available on the Reid Lab GitHub page (github.com/reidlab).

SUPPLEMENTAL MATERIAL

Supplemental material is available online only.

SUPPLEMENTAL FILE 1, PDF file, 1.4 MB.

ACKNOWLEDGMENTS

We thank R. Richardson for use of the Tecan plate reader and M. Pfeifer for assistance with fluorescence spectroscopy.

We declare that the research was conducted in the absence of any commercial or financial relationships that could be construed as a potential conflict of interest.

Funding was provided by the NSF Environmental Chemical Sciences program award number 1905175 to M.C.R. and by the NSERC discovery grant program to A.J.P. H.Y. was supported by a fellowship from the Cornell University Graduate School. This work made use of the Cornell Center for Materials Research Shared Facilities, which are supported through the NSF MRSEC program (DMR-1719875).

REFERENCES

- Abernathy CO, Liu YP, Longfellow D, Aposhian HV, Beck B, Fowler B, Goyer R, Menzer R, Rossman T, Thompson C, Waalkes M. 1999. Arsenic: health effects, mechanisms of actions, and research issues. Environ Health Perspect 107:593–597. https://doi.org/10.1289/ehp.99107593.
- Chappell W, Beck B, Brown K, Chaney R, Cothern R, Cothern C, Irgolic K, North D, Thornton I, Tsongas T. 1997. Inorganic arsenic: a need and an opportunity to improve risk assessment. Environ Health Perspect 105:1060–1067. https://doi.org/10.1289/ehp.971051060.
- Mendez WM, Eftim S, Cohen J, Warren I, Cowden J, Lee JS, Sams R. 2017. Relationships between arsenic concentrations in drinking water and lung and bladder cancer incidence in US counties. J Expo Sci Environ Epidemiol 27:235–243. https://doi.org/10.1038/jes.2016.58.
- Smith AH, Hopenhayn-Rich C, Bates MN, Goeden HM, Hertz-Picciotto I, Duggan HM, Wood R, Kosnett MJ, Smith MT. 1992. Cancer risks from arsenic in drinking water. Environ Health Perspect 97:259–267. https://doi .org/10.1289/ehp.9297259.
- Wasserman GA, Liu X, Parvez F, Factor-Litvak P, Kline J, Siddique AB, Shahriar H, Uddin MN, van Geen A, Mey JL, Balac O, Graziano JH. 2016. Child intelligence and reductions in water arsenic and manganese: a two-year follow-up study in Bangladesh. Environ Health Perspect 124:1114–1120. https://doi .org/10.1289/ehp.1509974.
- Jia Y, Huang H, Zhong M, Wang F-H, Zhang L-M, Zhu Y-G. 2013. Microbial arsenic methylation in soil and rice rhizosphere. Environ Sci Technol 47: 3141–3148. https://doi.org/10.1021/es303649v.
- Maguffin SC, Kirk MF, Daigle AR, Hinkle SR, Jin Q. 2015. Substantial contribution of biomethylation to aquifer arsenic cycling. Nature Geosci 8:290–293. https://doi.org/10.1038/ngeo2383.

- Zhu Y-G, Xue X-M, Kappler A, Rosen BP, Meharg AA. 2017. Linking genes to microbial biogeochemical cycling: lessons from arsenic. Environ Sci Technol 51:7326–7339. https://doi.org/10.1021/acs.est.7b00689.
- Chen C, Shen Y, Li Y, Zhang W, Zhao F-J. 2021. Demethylation of the antibiotic methylarsenite is coupled to denitrification in anoxic paddy soil. Environ Sci Technol 55:15484–15494. https://doi.org/10.1021/acs.est.1c04167.
- Jia Y, Huang H, Chen Z, Zhu Y-G. 2014. Arsenic uptake by rice is influenced by microbe-mediated arsenic redox changes in the rhizosphere. Environ Sci Technol 48:1001–1007. https://doi.org/10.1021/es403877s.
- Lomax C, Liu WJ, Wu L, Xue K, Xiong J, Zhou J, McGrath SP, Meharg AA, Miller AJ, Zhao FJ. 2012. Methylated arsenic species in plants originate from soil microorganisms. New Phytol 193:665–672. https://doi.org/10 .1111/j.1469-8137.2011.03956.x.
- Reid MC, Maillard J, Bagnoud A, Falquet L, Le Vo P, Bernier-Latmani R. 2017. Arsenic methylation dynamics in a rice paddy soil anaerobic enrichment culture. Environ Sci Technol 51:10546–10554. https://doi.org/10.1021/acs.est.7b02970.
- Viacava K, Meibom KL, Ortega D, Dyer S, Gelb A, Falquet L, Minton NP, Mestrot A, Bernier-Latmani R. 2020. Variability in arsenic methylation efficiency across aerobic and anaerobic microorganisms. Environ Sci Technol 54:14343–14351. https://doi.org/10.1021/acs.est.0c03908.
- Zhu Y-G, Yoshinaga M, Zhao F-J, Rosen BP. 2014. Earth abides arsenic biotransformations. Annu Rev Earth Planet Sci 42:443–467. https://doi.org/ 10.1146/annurev-earth-060313-054942.
- Pothier MP, Hinz AJ, Poulain AJ. 2018. Insights into arsenite and arsenate uptake pathways using a whole cell biosensor. Front Microbiol 9:2310. https://doi.org/10.3389/fmicb.2018.02310.

- Rosenberg H, Gerdes R, Chegwidden K. 1977. Two systems for the uptake of phosphate in *Escherichia coli*. J Bacteriol 131:505–511. https://doi.org/ 10.1128/jb.131.2.505-511.1977.
- 17. Willsky GR, Malamy MH. 1980. Characterization of two genetically separable inorganic phosphate transport systems in *Escherichia coli*. J Bacteriol 144:356–365. https://doi.org/10.1128/jb.144.1.356-365.1980.
- Willsky GR, Malamy MH. 1980. Effect of arsenate on inorganic phosphate transport in *Escherichia coli*. J Bacteriol 144:366–374. https://doi.org/10 .1128/jb.144.1.366-374.1980.
- Meng Y-L, Liu Z, Rosen BP. 2004. As(III) and Sb(III) uptake by GIpF and efflux by ArsB in *Escherichia coli*. J Biol Chem 279:18334–18341. https://doi.org/10.1074/jbc.M400037200.
- Rosen BP. 2002. Transport and detoxification systems for transition metals, heavy metals and metalloids in eukaryotic and prokaryotic microbes.
 Comp Biochem Physiol A Mol Integr Physiol 133:689–693. https://doi.org/10.1016/S1095-6433(02)00201-5.
- Sanders OI, Rensing C, Kuroda M, Mitra B, Rosen BP. 1997. Antimonite is accumulated by the glycerol facilitator GlpF in *Escherichia coli*. J Bacteriol 179:3365–3367. https://doi.org/10.1128/jb.179.10.3365-3367.1997.
- Spinello A, De Almeida A, Casini A, Barone G. 2016. The inhibition of glycerol permeation through aquaglyceroporin-3 induced by mercury(II): a molecular dynamics study. J Inorg Biochem 160:78–84. https://doi.org/10.1016/j.jinorgbio.2015.11.027.
- Wu B, Steinbronn C, Alsterfjord M, Zeuthen T, Beitz E. 2009. Concerted action of two cation filters in the aquaporin water channel. EMBO J 28: 2188–2194. https://doi.org/10.1038/emboj.2009.182.
- Bienert GP, Desguin B, Chaumont F, Hols P. 2013. Channel-mediated lactic acid transport: a novel function for aquaglyceroporins in bacteria. Biochem J 454:559–570. https://doi.org/10.1042/BJ20130388.
- Borgnia MJ, Kozono D, Calamita G, Maloney PC, Agre P. 1999. Functional reconstitution and characterization of AqpZ, the E. coli water channel protein. J Mol Biol 291:1169–1179. https://doi.org/10.1006/jmbi.1999.3032.
- Heller KB, Lin E, Wilson TH. 1980. Substrate specificity and transport properties of the glycerol facilitator of *Escherichia coli*. J Bacteriol 144:274–278. https://doi.org/10.1128/jb.144.1.274-278.1980.
- 27. Porquet A, Filella M. 2007. Structural evidence of the similarity of $Sb(OH)_3$ and $As(OH)_3$ with glycerol: implications for their uptake. Chem Res Toxicol 20:1269–1276. https://doi.org/10.1021/tx700110m.
- Aftabtalab A, Rinklebe J, Shaheen SM, Niazi NK, Moreno-Jiménez E, Schaller J, Knorr K-H. 2022. Review on the interactions of arsenic, iron (oxy)(hydr) oxides, and dissolved organic matter in soils, sediments, and groundwater in a ternary system. Chemosphere 286:131790. https://doi.org/10.1016/j .chemosphere.2021.131790.
- Mladenov N, Zheng Y, Miller MP, Nemergut DR, Legg T, Simone B, Hageman C, Rahman MM, Ahmed KM, McKnight DM. 2010. Dissolved organic matter sources and consequences for iron and arsenic mobilization in Bangladesh aquifers. Environ Sci Technol 44:123–128. https://doi.org/ 10.1021/es901472g.
- Weissenborn DL, Wittekindt N, Larson TJ. 1992. Structure and regulation of the glpFK operon encoding glycerol diffusion facilitator and glycerol kinase of Escherichia coli K-12. J Biol Chem 267:6122–6131. https://doi.org/ 10.1016/S0021-9258(18)42670-1.
- Buschmann J, Kappeler A, Lindauer U, Kistler D, Berg M, Sigg L. 2006. Arsenite and arsenate binding to dissolved humic acids: influence of pH, type of humic acid, and aluminum. Environ Sci Technol 40:6015–6020. https://doi.org/10.1021/es061057+.
- 32. Liu G, Fernandez A, Cai Y. 2011. Complexation of arsenite with humic acid in the presence of ferric iron. Environ Sci Technol 45:3210–3216. https://doi.org/10.1021/es102931p.
- Redman AD, Macalady DL, Ahmann D. 2002. Natural organic matter affects arsenic speciation and sorption onto hematite. Environ Sci Technol 36:2889–2896. https://doi.org/10.1021/es0112801.
- Ren J, Fan W, Wang X, Ma Q, Li X, Xu Z, Wei C. 2017. Influences of size-fractionated humic acids on arsenite and arsenate complexation and toxicity to *Daphnia magna*. Water Res 108:68–77. https://doi.org/10.1016/j.watres.2016 .10.052.
- 35. Chiasson-Gould SA, Blais JM, Poulain AJ. 2014. Dissolved organic matter kinetically controls mercury bioavailability to bacteria. Environ Sci Technol 48:3153–3161. https://doi.org/10.1021/es4038484.
- Graham AM, Cameron-Burr KT, Hajic HA, Lee C, Msekela D, Gilmour CC.
 2017. Sulfurization of dissolved organic matter increases Hg–sulfide–dissolved organic matter bioavailability to a Hg-methylating bacterium. Environ Sci Technol 51:9080–9088. https://doi.org/10.1021/acs.est.7b02781.

- 37. Hsu-Kim H, Kucharzyk KH, Zhang T, Deshusses MA. 2013. Mechanisms regulating mercury bioavailability for methylating microorganisms in the aquatic environment: a critical review. Environ Sci Technol 47:2441–2456. https://doi.org/10.1021/es304370g.
- Ndu U, Mason RP, Zhang H, Lin S, Visscher PT. 2012. Effect of inorganic and organic ligands on the bioavailability of methylmercury as determined by using a mer-lux bioreporter. Appl Environ Microbiol 78:7276–7282. https://doi .org/10.1128/AEM.00362-12.
- Al-Sid-Cheikh M, Pédrot M, Dia A, Guenet H, Vantelon D, Davranche M, Gruau G, Delhaye T. 2015. Interactions between natural organic matter, sulfur, arsenic and iron oxides in re-oxidation compounds within riparian wetlands: NanoSIMS and X-ray adsorption spectroscopy evidences. Sci Total Environ 515-516:118–128. https://doi.org/10.1016/j.scitotenv.2015.02.047.
- Guénet H, Davranche M, Vantelon D, Bouhnik-Le Coz M, Jardé E, Dorcet V, Demangeat E, Jestin J. 2017. Highlighting the wide variability in arsenic speciation in wetlands: a new insight into the control of the behavior of arsenic. Geochim Cosmochim Acta 203:284–302. https://doi.org/10.1016/ j.gca.2017.01.013.
- 41. Catrouillet C, Davranche M, Dia A, Bouhnik-Le Coz M, Pédrot M, Marsac R, Gruau G. 2015. Thiol groups controls on arsenite binding by organic matter: new experimental and modeling evidence. J Colloid Interface Sci 460: 310–320. https://doi.org/10.1016/j.jcis.2015.08.045.
- Hoffmann M, Mikutta C, Kretzschmar R. 2012. Bisulfide reaction with natural organic matter enhances arsenite sorption: insights from X-ray absorption spectroscopy. Environ Sci Technol 46:11788–11797. https://doi.org/10.1021/es302590x.
- 43. Langner P, Mikutta C, Kretzschmar R. 2012. Arsenic sequestration by organic sulphur in peat. Nat Geosci 5:66–73. https://doi.org/10.1038/ngeo1329.
- 44. Spuches AM, Kruszyna HG, Rich AM, Wilcox DE. 2005. Thermodynamics of the As(III)— thiol interaction: arsenite and monomethylarsenite complexes with glutathione, dihydrolipoic acid, and other thiol ligands. Inorg Chem 44:2964–2972. https://doi.org/10.1021/ic048694q.
- 45. Scott N, Hatlelid KM, MacKenzie NE, Carter DE. 1993. Reactions of arsenic(III) and arsenic(V) species with glutathione. Chem Res Toxicol 6:102–106. https://doi.org/10.1021/tx00031a016.
- Shen S, Li X-F, Cullen WR, Weinfeld M, Le XC. 2013. Arsenic binding to proteins. Chem Rev 113:7769–7792. https://doi.org/10.1021/cr300015c.
- Schmöger ME, Oven M, Grill E. 2000. Detoxification of arsenic by phytochelatins in plants. Plant Physiol 122:793–802. https://doi.org/10.1104/pp 122.3.793
- 48. Huang J-H. 2014. Impact of microorganisms on arsenic biogeochemistry: a review. Water Air Soil Pollut 225:1848. https://doi.org/10.1007/s11270-013-1848-v.
- 49. Rosen BP. 2002. Biochemistry of arsenic detoxification. FEBS Lett 529: 86–92. https://doi.org/10.1016/s0014-5793(02)03186-1.
- Buffi N, Merulla D, Beutier J, Barbaud F, Beggah S, Van Lintel H, Renaud P, van der Meer JR. 2011. Development of a microfluidics biosensor for agarose-bead immobilized *Escherichia coli* bioreporter cells for arsenite detection in aqueous samples. Lab Chip 11:2369–2377. https://doi.org/10.1039/c1lc20274j.
- Truffer F, Buffi N, Merulla D, Beggah S, Van Lintel H, Renaud P, van der Meer JR, Geiser M. 2014. Compact portable biosensor for arsenic detection in aqueous samples with *Escherichia coli* bioreporter cells. Rev Sci Instrum 85:e015120. https://doi.org/10.1063/1.4863333.
- Fang Y, Zhu C, Chen X, Wang Y, Xu M, Sun G, Guo J, Yoo J, Tie C, Jiang X, Li X. 2018. Copy number of ArsR reporter plasmid determines its arsenite response and metal specificity. Appl Microbiol Biotechnol 102:5753–5761. https://doi.org/10.1007/s00253-018-9042-1.
- Kostal J, Yang R, Wu CH, Mulchandani A, Chen W. 2004. Enhanced arsenic accumulation in engineered bacterial cells expressing ArsR. Appl Environ Microbiol 70:4582–4587. https://doi.org/10.1128/AEM.70.8.4582-4587.2004.
- Berset Y, Merulla D, Joublin A, Hatzimanikatis V, Van Der Meer JR. 2017.
 Mechanistic modeling of genetic circuits for ArsR arsenic regulation. ACS
 Synth Biol 6:862–874. https://doi.org/10.1021/acssynbio.6b00364.
- Jia X, Bu R, Zhao T, Wu K. 2019. Sensitive and specific whole-cell biosensor for arsenic detection. Appl Environ Microbiol 85:e00694-19. https://doi .org/10.1128/AEM.00694-19.
- Cortés-Salazar F, Beggah S, van der Meer JR, Girault HH. 2013. Electrochemical As(III) whole-cell based biochip sensor. Biosens Bioelectron 47: 237–242. https://doi.org/10.1016/j.bios.2013.03.011.
- Gudlavalleti RH, Bose SC, Verma SK, Khatri P, Scaria J, Dhewa S, Chaubey VK.
 A novel fluorometric bio-sensing-based arsenic detection system for groundwater. IEEE Sensors J 17:5391–5398. https://doi.org/10.1109/JSEN.2017 .2724200.

- Siddiki MSR, Kawakami Y, Ueda S, Maeda I. 2011. Solid phase biosensors for arsenic or cadmium composed of a trans factor and cis element complex. Sensors (Basel) 11:10063–10073. https://doi.org/10.3390/s111110063.
- Schweizer H. 1991. Escherichia-Pseudomonas shuttle vectors derived from pUC18/19. Gene 97:109–112. https://doi.org/10.1016/0378-1119(91)90016-5.
- 60. Alon U. 2019. An introduction to systems biology: design principles of biological circuits. CRC Press, Boca Raton, FL.
- Giometto A, Nelson DR, Murray AW. 2018. Physical interactions reduce the power of natural selection in growing yeast colonies. Proc Natl Acad Sci U S A 115:11448–11453. https://doi.org/10.1073/pnas.1809587115.
- Raab A, Feldmann J, Meharg AA. 2004. The nature of arsenic-phytochelatin complexes in *Holcus lanatus* and *Pteris cretica*. Plant Physiol 134:1113–1122. https://doi.org/10.1104/pp.103.033506.
- Abu-Ali L, Yoon H, Reid MC. 2022. Effects of organic sulfur and arsenite/dissolved organic matter ratios on arsenite complexation with dissolved organic matter. Chemosphere 302:134770. https://doi.org/10.1016/j.chemosphere .2022.134770.
- 64. Haitzer M, Aiken GR, Ryan JN. 2002. Binding of mercury(II) to dissolved organic matter: the role of the mercury-to-DOM concentration ratio. Environ Sci Technol 36:3564–3570. https://doi.org/10.1021/es025699i.
- 65. Stumm W, Morgan JJ. 2012. Aquatic chemistry: chemical equilibria and rates in natural waters. John Wiley & Sons, New York, NY.
- Borgnia M, Nielsen S, Engel A, Agre P. 1999. Cellular and molecular biology of the aquaporin water channels. Annu Rev Biochem 68:425–458. https://doi.org/10.1146/annurev.biochem.68.1.425.
- Joe-Wong C, Shoenfelt E, Hauser EJ, Crompton N, Myneni SC. 2012. Estimation of reactive thiol concentrations in dissolved organic matter and bacterial cell membranes in aquatic systems. Environ Sci Technol 46: 9854–9861. https://doi.org/10.1021/es301381n.
- Mangal V, Guéguen C. 2015. Examining concentrations and molecular weights of thiols in microorganism cultures and in Churchill River (Manitoba) using a fluorescent-labeling method coupled to asymmetrical flow field-flow fractionation. Anal Bioanal Chem 407:4305–4313. https://doi .org/10.1007/s00216-015-8599-0.
- Maguffin SC, Abu-Ali L, Tappero RV, Pena J, Rohila JS, McClung AM, Reid MC. 2020. Influence of manganese abundances on iron and arsenic solubility in rice paddy soils. Geochim Cosmochim Acta 276:50–69. https://doi .org/10.1016/j.gca.2020.02.012.
- Drexel RT, Haitzer M, Ryan JN, Aiken GR, Nagy KL. 2002. Mercury(II) sorption to two Florida Everglades peats: evidence for strong and weak binding and competition by dissolved organic matter released from the peat. Environ Sci Technol 36:4058–4064. https://doi.org/10.1021/es0114005.
- Skyllberg U, Drott A. 2010. Competition between disordered iron sulfide and natural organic matter associated thiols for mercury(II)—an EXAFS study. Environ Sci Technol 44:1254–1259. https://doi.org/10.1021/es902091w.
- Song Y, Jiang T, Liem-Nguyen V, Sparrman T, Björn E, Skyllberg U. 2018. Thermodynamics of Hg(II) bonding to thiol groups in Suwannee River natural organic matter resolved by competitive ligand exchange, Hg L_{III}-edge EXAFS and ¹H NMR spectroscopy. Environ Sci Technol 52:8292–8301. https://doi.org/10.1021/acs.est.8b00919.
- Skyllberg U, Qian J, Frech W. 2005. Combined XANES and EXAFS study on the bonding of methyl mercury to thiol groups in soil and aquatic organic matter. Phys Scr 2005:894. https://doi.org/10.1238/Physica.Topical.115a00894.
- Jensen MØ, Park S, Tajkhorshid E, Schulten K. 2002. Energetics of glycerol conduction through aquaglyceroporin GlpF. Proc Natl Acad Sci U S A 99: 6731–6736. https://doi.org/10.1073/pnas.102649299.
- Song J, Almasalmeh A, Krenc D, Beitz E. 2012. Molar concentrations of sorbitol and polyethylene glycol inhibit the Plasmodium aquaglyceroporin but not that of *E. coli*: involvement of the channel vestibules. Biochim Biophys Acta 1818:1218–1224. https://doi.org/10.1016/j.bbamem.2012.01.025.
- Stülke J, Hillen W. 1999. Carbon catabolite repression in bacteria. Curr Opin Microbiol 2:195–201. https://doi.org/10.1016/S1369-5274(99)80034-4.
- Hoffmann M, Mikutta C, Kretzschmar R. 2013. Arsenite binding to natural organic matter: spectroscopic evidence for ligand exchange and ternary complex formation. Environ Sci Technol 47:12165–12173. https://doi.org/ 10.1021/es4023317.
- Baumann B, van der Meer JR. 2007. Analysis of bioavailable arsenic in rice with whole cell living bioreporter bacteria. J Agric Food Chem 55:2115–2120. https://doi.org/10.1021/jf0631676.

- Luo C, Walk ST, Gordon DM, Feldgarden M, Tiedje JM, Konstantinidis KT.
 2011. Genome sequencing of environmental *Escherichia coli* expands understanding of the ecology and speciation of the model bacterial species. Proc Natl Acad Sci U S A 108:7200–7205. https://doi.org/10.1073/pnas.1015622108
- Dixit S, Hering JG. 2003. Comparison of arsenic(V) and arsenic(III) sorption onto iron oxide minerals: implications for arsenic mobility. Environ Sci Technol 37:4182–4189. https://doi.org/10.1021/es030309t.
- 81. Zhao F-J, Zhu Y-G, Meharg AA. 2013. Methylated arsenic species in rice: geographical variation, origin, and uptake mechanisms. Environ Sci Technol 47:3957–3966. https://doi.org/10.1021/es304295n.
- 82. Bhattacharjee H, Mukhopadhyay R, Thiyagarajan S, Rosen BP. 2008. Aquaglyceroporins: ancient channels for metalloids. J Biol 7:33–36. https://doi.org/10.1186/jbiol91.
- 83. Stroud RM, Miercke LJ, O'Connell J, Khademi S, Lee JK, Remis J, Harries W, Robles Y, Akhavan D. 2003. Glycerol facilitator GlpF and the associated aquaporin family of channels. Curr Opin Struct Biol 13:424–431. https://doi.org/10.1016/S0959-440X(03)00114-3.
- Zhao FJ, Ma JF, Meharg A, McGrath S. 2009. Arsenic uptake and metabolism in plants. New Phytol 181:777–794. https://doi.org/10.1111/j.1469-8137.2008.02716.x.
- Hebisch E, Knebel J, Landsberg J, Frey E, Leisner M. 2013. High variation of fluorescence protein maturation times in closely related *Escherichia coli* strains. PLoS One 8:e75991. https://doi.org/10.1371/journal.pone.0075991.
- 86. Maye P, Fu Y, Butler DL, Chokalingam K, Liu Y, Floret J, Stover ML, Wenstrup R, Jiang X, Gooch C, Rowe D. 2011. Generation and characterization of *Col10a1*-mcherry reporter mice. Genesis 49:410–418. https://doi.org/10.1002/dvg.20733.
- 87. Neidhardt FC, Curtiss R, III, Ingraham JL, Lin ECC, Low KB, Magasanik B, Reznikoff WS, Riley M, Schaechter M, Umbarger HE (ed). 1996. Escherichia coli and Salmonella: cellular and molecular biology. ASM Press, Washington, DC.
- 88. Ramanathan S, Shi W, Rosen BP, Daunert S. 1997. Sensing antimonite and arsenite at the subattomole level with genetically engineered bioluminescent bacteria. Anal Chem 69:3380–3384. https://doi.org/10.1021/ac970111p.
- 89. Xu C, Rosen BP. 1997. Dimerization is essential for DNA binding and repression by the ArsR metalloregulatory protein of *Escherichia coli*. J Biol Chem 272:15734–15738. https://doi.org/10.1074/jbc.272.25.15734.
- Busenlehner LS, Pennella MA, Giedroc DP. 2003. The SmtB/ArsR family of metalloregulatory transcriptional repressors: structural insights into prokaryotic metal resistance. FEMS Microbiol Rev 27:131–143. https://doi .org/10.1016/S0168-6445(03)00054-8.
- 91. Stocker J, Balluch D, Gsell M, Harms H, Feliciano J, Daunert S, Malik KA, Van der Meer JR. 2003. Development of a set of simple bacterial biosensors for quantitative and rapid measurements of arsenite and arsenate in potable water. Environ Sci Technol 37:4743–4750. https://doi.org/10.1021/es034258b.
- 92. R Core Team. 2013. R: a language and environment for statistical computing. R Foundation for Statistical Computing, Vienna, Austria.
- IHSS. 2016. Elemental compositions and stable isotopic ratios of IHSS samples. https://humic-substances.org/elemental-compositions-and-stable-isotopic-ratios-of-ihss-samples/.
- 94. Reid MC, Asta MP, Falk L, Maguffin SC, Pham VHC, Le HA, Bernier-Latmani R, Le Vo P. 2021. Associations between inorganic arsenic in rice and groundwater arsenic in the Mekong Delta. Chemosphere 265:129092. https://doi.org/10.1016/j.chemosphere.2020.129092.
- 95. Zhang X, Reid MC. 2022. Inhibition of methanogenesis leads to accumulation of methylated arsenic species and enhances arsenic volatilization from rice paddy soil. Sci Total Environ 818:151696. https://doi.org/10.1016/j.scitotenv.2021.151696.
- McGuffie MJ, Barrick JE. 2021. pLannotate: engineered plasmid annotation. Nucleic Acids Res 49:W516–W522. https://doi.org/10.1093/nar/gkab374.
- 97. Holm S. 1979. A simple sequentially rejective multiple test procedure. Scand J Stat:65–70.
- Shao B, Rammohan J, Anderson DA, Alperovich N, Ross D, Voigt CA. 2021.
 Single-cell measurement of plasmid copy number and promoter activity.
 Nat Commun 12:1475. https://doi.org/10.1038/s41467-021-21734-y.
- 99. Konovalova A, Schwalm JA, Silhavy TJ. 2016. A suppressor mutation that creates a faster and more robust σE envelope stress response. J Bacteriol 198:2345–2351. https://doi.org/10.1128/JB.00340-16.